Inorganic Chemistry

Article

pubs.acs.org/IC

Infrared Vibrational Spectroscopy of $[Ru(bpy)_2(bpm)]^{2+}$ and $[Ru(bpy)_3]^{2+}$ in the Excited Triplet State

Tatsuhiko Mukuta,[†] Naoto Fukazawa,[†] Kei Murata,[‡] Akiko Inagaki,[§,∥] Munetaka Akita,[‡] Sei'ichi Tanaka,[†] Shin-ya Koshihara,[†] and Ken Onda*[,⊥,∥]

[†]Department of Chemistry and Materials Science, Tokyo Institute of Technology, O-okayama, Meguro-ku, Tokyo 152-8551, Japan

[‡]Chemical Resources Laboratory, Tokyo Institute of Technology, 4259 Nagatsuta, Midori-ku, Yokohama 226-8503, Japan

[§]Graduate School of Science and Engineering, Tokyo Metropolitan University, 1-1 minami-Osawa, Hachioji, Tokyo 192-0397, Japan

[⊥]Interactive Research Center of Science, Tokyo Institute of Technology, Nagatsuta, Midori-ku, Yokohama, Kanagawa 226-8502, Japan

[∥]PRESTO, Japan Science and Technology Agency (JST), 4-1-8 Honcho, Kawaguchi, Saitama 332-0012, Japan

Supporting Information

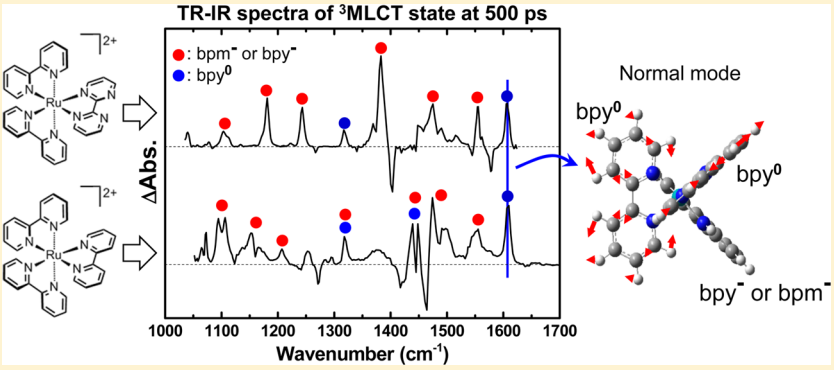

ABSTRACT: This work involved a detailed investigation into the infrared vibrational spectra of ruthenium polypyridyl complexes, specifically heteroleptic $[Ru(bpy)_2(bpm)]^{2+}$ (bpy = 2,2′-bipyridine and bpm = 2,2′-bipyrimidine) and homoleptic $[Ru(bpy)_3]^{2+}$, in the excited triplet state. Transient spectra were acquired 500 ps after photoexcitation, corresponding to the vibrational ground state of the excited triplet state, using time-resolved infrared spectroscopy. We assigned the observed bands to specific ligands in $[Ru(bpy)_2(bpm)]^{2+}$ based on the results of deuterium substitution and identified the corresponding normal vibrational modes using quantum-chemical calculations. Through this process, the more complex vibrational bands of $[Ru(bpy)_3]^{2+}$ were assigned to normal vibrational modes. The results are in good agreement with the model in which excited electrons are localized on a single ligand. We also found that the vibrational bands of both complexes associated with the ligands on which electrons are little localized appear at approximately 1317 and 1608 cm^{-1}. These assignments should allow the study of the reaction dynamics of various photofunctional systems including ruthenium polypyridyl complexes.

I. INTRODUCTION

Ruthenium(II) polypyridyl complexes are widely used in photofunctional systems, such as photocatalysts and organic solar cells, as well as in biophysical applications, because they exhibit significant absorption over a wide range of visible light. Such absorption allows the efficient generation of an excited triplet state with a lifetime of more than 100 ns.[1−10] Recently, the application of these materials as visible-light photoredox catalysts has also attracted the attention of groups working in the field of organic synthesis.[11−13] If the excited complexes can be followed in real time during these photochemical processes, this becomes a powerful tool for understanding their mechanisms, as well as for designing new systems. Unfortunately, the complicated electronic structures and dynamics associated with the excited states of coordination metal complexes make it difficult to perform such analyses.

One of the best means of solving this problem is time-resolved infrared (TR-IR) vibrational spectroscopy.[14,15] In this method, a metal complex is excited by an ultrashort pulse of visible light, following which IR absorption spectra are measured after a specific time delay, using an ultrashort IR pulse. In this manner, vibrational spectra of the excited states can be obtained straightforwardly, allowing ready examination of the electronic structures and dynamics in the excited state by analysis of the transient spectra. Moreover, because only signals modulated by the pump pulse are detected, information

Received: September 30, 2013
Published: February 14, 2014

 © 2014 American Chemical Society dx.doi.org/10.1021/ic402474t | Inorg. Chem. 2014, 53, 2481−2490

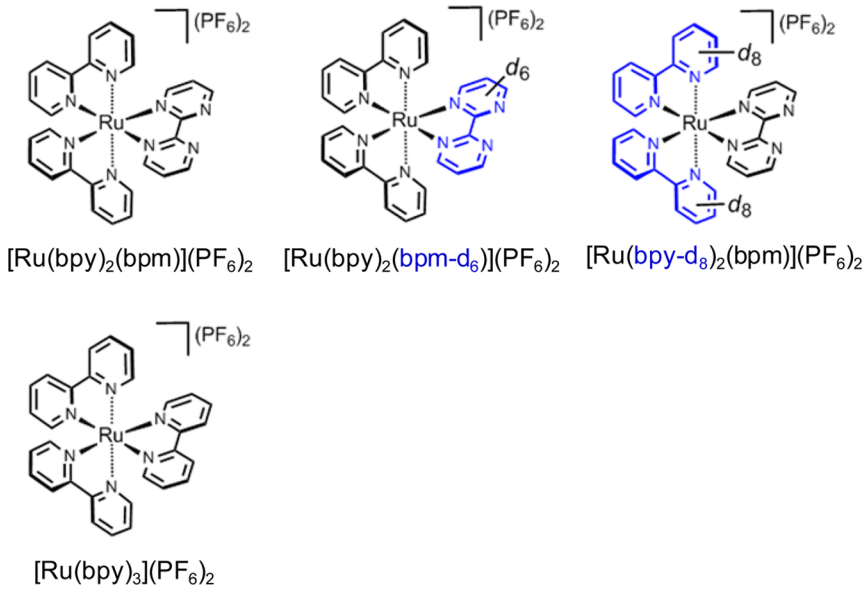

Figure 1. Molecular structures of the complexes investigated.

Scheme 1

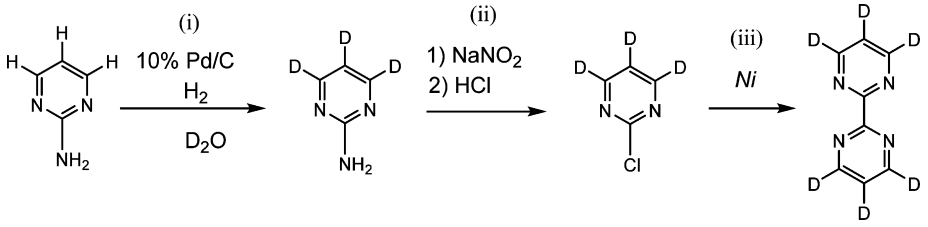

concerning the complex of interest is selectively obtained, even in the presence of a solvent and other reactants having strong IR absorption, by employing a high-intensity IR laser in conjunction with a high-sensitivity detector.

To date, this method has been applied primarily to coordination metal complexes with simple ligands that exhibit strong IR absorption, such as CO and CN.[14,15] In order to apply this method to a wider range of complexes, it is necessary to be able to observe more complex ligands, such as polypyridyl moieties. The C═C and C═N double bonds present in such ligands are very sensitive to variations in charge and structure during photoexcitation and thus represent a useful mechanism for probing electronic structures and dynamics in the excited state.[16−18]

Several studies of the IR vibrational spectra of such ligands in the excited state using TR-IR spectroscopy have been reported,[14,15,19−25] but the vibrational mode assignments in these studies have been either incomplete or simplified. For this reason, we undertook the comprehensive study of the IR vibrational spectra of polypyridyl ligands in excited-state ruthenium(II) polypyridyl complexes. We chose homoleptic $[Ru(bpy)_3]^{2+}$ (bpy = 2,2′-bipyridine) and heteroleptic $[Ru(bpy)_2(bpm)]^{2+}$ (bpm = 2,2′-bipyrimidine) shown in Figure 1 and acquired their vibrational spectra in the metastable excited triplet state using high-sensitivity TR-IR. $[Ru(bpy)_3]^{2+}$ is prototypical and the most studied ruthenium polypyridyl complex, whereas no TR vibrational spectrum of $[Ru(bpy)_2(bpm)]^{2+}$ has been measured, despite it differing from $[Ru(bpy)_3]^{2+}$ by only one ligand and the fact that its derivatives show interesting photochemical and photophysical phenomena.[4,26] We assigned the observed vibrational bands to normal vibrational modes obtained from quantum-chemical calculations, applying data obtained from deuterium substitution studies.

Quantum-chemical calculations based on the density functional theory (DFT) method are a powerful means of elucidating the molecular and electronic structures of various transition-metal complexes. However, it remains difficult to precisely describe the excited states of complicated molecules using DFT, so we therefore initially studied heteroleptic $[Ru(bpy)_2(bpm)]^{2+}$ because its asymmetric structure results in a simpler vibrational spectrum. By comparing the experimental spectra obtained for deuterated complexes with the simulated spectra derived from DFT calculations, we confirmed the validity of the calculations. On the basis of these results, we went on to examine $[Ru(bpy)_3]^{2+}$, which generates more complex vibrational spectra because of its higher symmetry. As a result, we succeeded in assigning almost all of the observed vibrational bands associated with the bpy and bpm ligands over the range of 1000−1700 cm^{-1}. These assignments should become a powerful tool for studying general ruthenium polypyridyl complexes during various photochemical processes.

II. EXPERIMENTAL SECTION

II.1. Materials. *II.1.1. Synthesis of Deuterated Ligands.* The syntheses of 2-aminopyrimidine-d_3[27] and 2-chloropyrimidine-d_3[28] were carried out following reported procedures, as shown in Scheme 1, steps I and ii (2-aminopyrimidine-d_3, 72% yield, m/z 98; 2-chloropyrimidine-d_3, 30%, m/z 117). The synthesis of 2,2′-bipyrimidine-d_6 was performed using a standard nickel coupling reaction[29] with 2-chloropyrimidine-d_3, as shown in Scheme 1, step iii,

dx.doi.org/10.1021/ic402474t | Inorg. Chem. 2014, 53, 2481−2490

to yield the desired product (37%, m/z 164). Deuterated 2,2′-bipyridine (2,2′-bipyridine-d_8) was also synthesized, as described in refs 27 and30 (88%, m/z 164).

II.1.2. Synthesis of [Ru(bpy)$_2$(bpm)](PF$_6$)$_2$ and Its Deuterated Complexes.[31−33] The mononuclear ruthenium complexes [Ru(bpy-d_m)$_2$(bpm-d_n)](PF$_6$)$_2$ were synthesized using the deuterated 2,2′-bipyridyls and bipyrimidines, following previously published methods (eq 1).

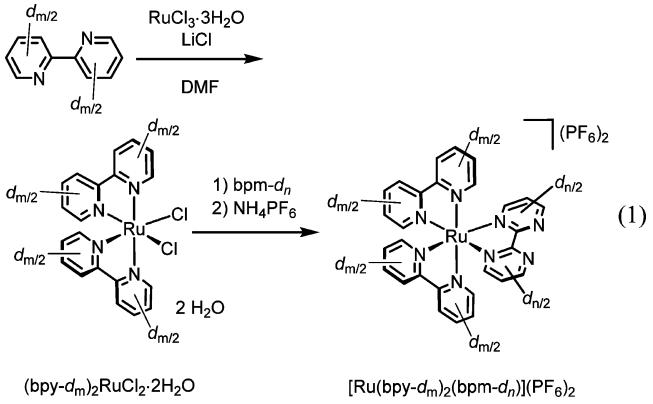

(1)

II.1.3. Evaluation of the D Content of the Deuterated Complexes. The D content in the deuterated complexes [Ru(bpy-h_8)$_2$(bpm-d_n)](PF$_6$)$_2$ and [Ru(bpy-d_m)$_2$(bpm-h_6)](PF$_6$)$_2$ was evaluated using ^{1}H NMR and electrospray ionization mass spectrometry (ESI-MS) spectral data. In the ^{1}H NMR spectra of the ruthenium compounds, the integral intensity of the nondeuterated ligand was used as an internal standard to estimate the D content of the deuterated ligand. Thus, in [Ru(bpy-h_8)$_2$(bpm-d_n)](PF$_6$)$_2$, bipyridyl signals and their integral intensities were used to evaluate the D content of the bpm-d_n ligand (74%). Similarly, the D content of the deuterated bpm ligand was estimated to be 98% in [Ru(bpy-d_m)$_2$(bpm-h_6)](PF$_6$)$_2$. The D content value was also supported by the ESI-MS spectral data. These spectra are shown in the Supporting Information (SI; Figure S1).

II.2. Instrumentation. IR vibrational spectra in the excited state were acquired by the pump−probe method. The details of the experimental setup have already been reported in a previous paper and so are only described briefly here.[16,18,25] A mid-IR probe pulse was generated using a combination of optical parametric amplification and difference frequency generation applied to the output of a femtosecond Ti:sapphire amplifier (pulse duration = 120 fs, wavelength = 800 nm, and repetition rate = 1 kHz). The bandwidth and tunable range of the IR pulse were 150 and 1000−3700 cm^{-1}, respectively, and the 400 nm pump pulse was obtained by doubling the output of the amplifier. The sample solution flowed through an IR cell equipped with BaF_2 windows with an optical path length of 0.1 mm. Typical diameter and pulse energy values were 350 μm and 17 μJ pulse^{-1} (∼18 mJ cm^{-2}) for the pump pulse and 150 μm and 0.2 μJ pulse^{-1} for the probe pulse. The linearity was checked by plotting the spectral change as a function of the pump pulse fluence, as shown in Figure S2 in the SI. The probe pulse passed through the IR cell and was subsequently dispersed by a 19 cm polychromator and acquired with a 64-channel mercury−cadmium−telluride (MCT) IR detector array. The laser apparatus was carefully adjusted prior to each measurement so as to obtain the optimal signal-to-noise (S/N) ratio. Each sample solution was prepared at a concentration of 1 mM acetonitrile, and measurements were conducted in air. The typical absorbance change (ΔAbs) was 5×10^{-4}, and the noise level was less than 1×10^{-5}. The pronounced IR absorption of the solvent precluded the acquisition of the vibrational spectra of ground-state complexes in solution, and thus we prepared KBr pellets incorporating a small amount of the sample and acquired the IR spectra of the resulting specimens using a commercial Fourier transform infrared (FT-IR) spectrometer. By comparing the ground-state spectra of the KBr pellet samples measured using the MCT array and FT-IR, we were able to calibrate the pump−probe system and determined a wavelength accuracy of ±1 cm^{-1}.

II.3. Quantum-Chemical Calculations. All calculations were performed at the DFT level using the *Gaussian 09* package.[34] The geometry optimizations were performed using the *mPW1PW91* functional.[35] and the LanL2DZ basis set was employed for all atoms and extended by a polarization function (except for hydrogen).[36−38] The lowest triplet excited states were optimized with the unrestricted DFT (UmPW1PW91). To address solvation effects, the polarizable continuum model[39] was used for the lowest triplet excited states. Frequency calculations were then performed to confirm the optimized structures to be an energy minimum and obtain vibrational spectra (frequencies scaled by 0.97). The comparison of the vibrational spectra using different methods together with the experimental spectra is shown in Figure S3 in the SI. The orbital plots, as well as the graphical representations, were generated using *Molekel*.[40] The total zero-point energies and Cartesian coordinates of the computed structures are given in Tables S1 and S2 in the SI. Time-dependent DFT (TD-DFT) calculations were performed to investigate the vertical excitations. Both lower singlet and triplet excited states were considered in the calculations.

III. RESULTS AND DISCUSSION

III.1. [Ru(bpy)$_2$(bpm)]$^{2+}$ and Its Deuterated Complexes. *III.1.1. Vibrational Bands of the Ground and Excited Triplet States.* Figure 2a shows the IR absorption spectra of KBr pellets of [Ru(bpy)$_2$(bpm)](PF$_6$)$_2$ and its deuterated complexes, [Ru(bpy)$_2$(bpm-d_6)](PF$_6$)$_2$ and [Ru(bpy-d_8)$_2$(bpm)](PF$_6$)$_2$, in the ground state, acquired using FT-IR spectroscopy. If a normal vibrational mode consists of only vibrations of the bpy ligand, its energy is significantly shifted by deuteration of the bpy ligand but not changed by deuteration of the bpm ligand, and vice versa. Thus, one can judge which ligand, bpy or bpm, a vibrational band should be assigned to by comparing these three spectra. As shown in Figure 2a, there were no changes in the three bands at 1407, 1545, or 1577 cm^{-1} following deuteration of the bpy ligand (bpy-d_8); by contrast, these bands are not present subsequent to deuteration of the bpm ligand (bpm-d_6). These three bands are consequently assigned to vibrational modes localized at the bpm ligands, as indicated by red solid circles in Figure 2a. In the same manner, the nine bands at 1124, 1163, 1244, 1275, 1315, 1427, 1448, 1468, and 1606 cm^{-1} were assigned to vibrational modes localized at the bpy ligands and are indicated by blue solid circles.

This procedure was also applied to the assignments of the vibrational bands of the triplet excited state in the CH_3CN solutions of these three complexes. Figure 2b shows the absorption change spectra of these three complexes 500 ps after photoexcitation with a 400 nm pulse. In general, ruthenium polypyridyl complexes are known to be the vibrational ground state in the long-lived triplet state at this point in time.[1−3] Both positive and negative peaks are evident in these spectra; the positive peaks are attributed to transitions from the vibrational ground state ($v = 0 \rightarrow v = 1$) of the excited triplet state, whereas the negative peaks correspond to bleaching of the vibrational transition in the ground state because the population of the ground state is reduced by photoexcitation.

The six positive bands at 1104, 1182, 1243, 1383, 1475, and 1554 cm^{-1} are unaffected by deuteration of the bpy ligand but disappear following deuteration of the bpm ligand, and so these bands are assigned to vibrational modes localized at the bpm ligands. In contrast, the two positive bands at 1318 and 1607 cm^{-1} are assigned to vibrational modes localized at the bpy ligands. The three negative bands at 1402, 1544, and 1578 cm^{-1}

dx.doi.org/10.1021/ic402474t | Inorg. Chem. 2014, 53, 2481−2490

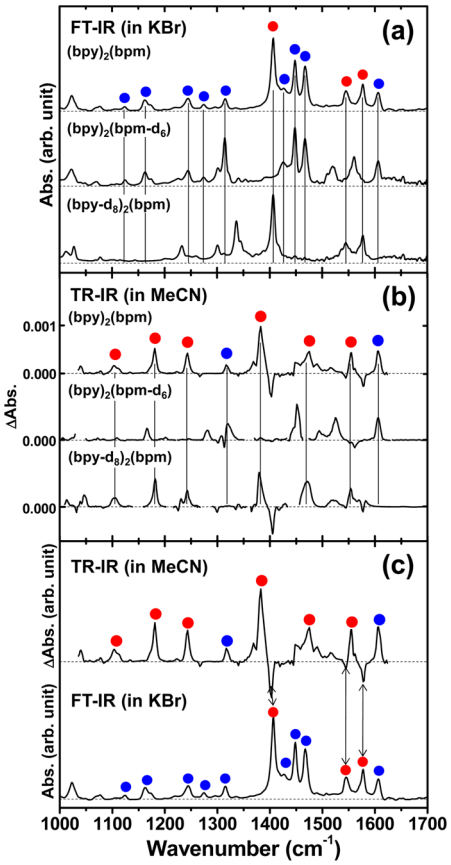

Figure 2. IR vibrational spectra of $[Ru(bpy)_2(bpm)]^{2+}$ and its deuterated analogues, $[Ru(bpy)_2(bpm\text{-}d_6)]^{2+}$ and $[Ru(bpy\text{-}d_8)_2(bpm)]^{2+}$: (a) FT-IR spectra of the complexes as KBr pellets; (b) TR-IR spectra of CH_3CN solutions of the complexes 500 ps after photoexcitation with a 400 nm pulse; (c) comparison of the FT-IR and TR-IR spectra of $[Ru(bpy)_2(bpm)]^{2+}$. The red and blue circles represent bands associated with vibrations localized at the bpm and bpy ligands, respectively, based on wavenumber shifts following deuterium substitution, as detailed in the text.

are changed only by deuteration of the bpm ligand and so must be due to vibrational modes of the bpm ligands. This result is consistent with the observation that the positions of these negative bands correspond to those of the peaks assigned to the bpm ligands in the ground state, as shown in Figure 2c. The slight differences in wavenumbers between the bleach and TR-IR bands are presumably due to solvation effects.

On the basis of the above assignments resulting from deuterium substitution studies, several general characteristics of the vibrational spectra are derived. First, it appears that the majority of the vibrational bands in the ground state are assigned to the bpy ligand, whereas most of the bands in the excited state are associated with the bpm ligands. In addition, all of the negative bands can be assigned to the bpm vibrational modes. These findings are explained by the model that the excited electrons are primarily localized on the bpm ligands, meaning that photoexcitation of these compounds results in electron transfer from the metal to the bpm ligands. This is in good agreement with the results of the electrochemical measurements.[41]

III.1.2. Normal Vibrational Modes by Quantum-Chemical Calculations. To assign the observed vibrational bands to the normal vibrational modes of the complex, we compared the experimentally derived spectra to the results of the DFT calculations, taking into account the above assignments based on deuterium substitution. Figure 3a compares the observed

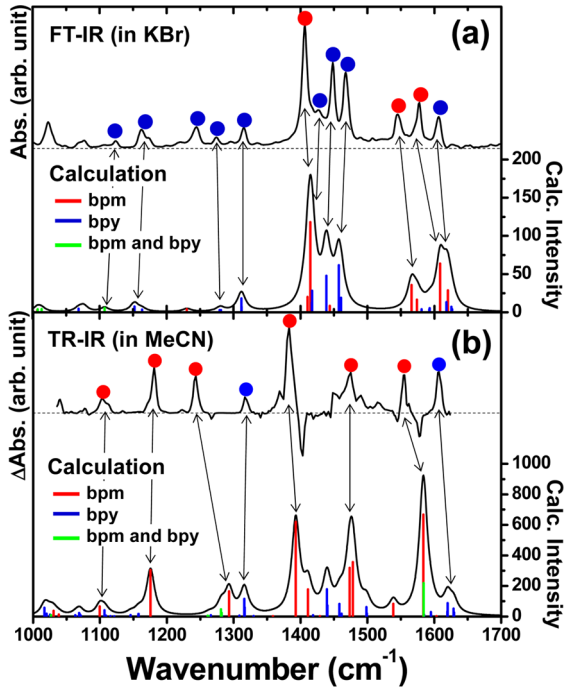

Figure 3. Comparison of the observed and calculated vibrational spectra of $[Ru(bpy)_2(bpm)]^{2+}$: (a) experimental FT-IR spectrum (upper) and calculated S_0 state spectrum (lower); (b) experimental TR-IR spectrum (upper) and calculated T_1 state spectrum (lower). The bars in the experimental spectra provide the wavenumber and intensity of each vibrational mode, and their colors indicate the ligand on which the vibrations are localized, based on the displacement of each normal vibrational mode obtained from calculations (Figures 4 and 5). Color code: blue, bpy; red, bpm; green, both ligands.

FT-IR spectrum and the calculated spectrum of ground-state (S_0) $[Ru(bpy)_2(bpm)]^{2+}$. The wavenumbers and intensities of the colored bars correspond to the values derived for normal modes via calculations, while the color of each bar indicates the ligand to which each mode belongs. The blue and red bars represent the modes associated with bond vibrations in the bpy and bpm ligands, respectively, while the green bars represent the modes associated with both the bpy and bpm ligands. These assignments are based on the vibrational motions obtained from the quantum-chemical calculation results shown in Figure 4. The convoluted spectra were obtained from a Lorentzian function with a 15 cm^{-1} bandwidth (fwhm) along with the calculated intensity at each wavenumber.

Although the convoluted vibrational bands are composed of several normal vibrational mode peaks, each band can be assigned to a single main vibrational mode, and the experimentally observed bands are well matched by the calculation results. We therefore assigned each observed band to a calculated band, by considering to which ligand each vibrational band belongs, as shown in Figure 3a. The correspondences between the observed and calculated bands together with their normal modes are also summarized in Figure 4. It is noted that the vibrational spectra of the deuterated complexes should be reproduced by the same calculation considering deuteration; however, they did not

dx.doi.org/10.1021/ic402474t | Inorg. Chem. 2014, 53, 2481−2490

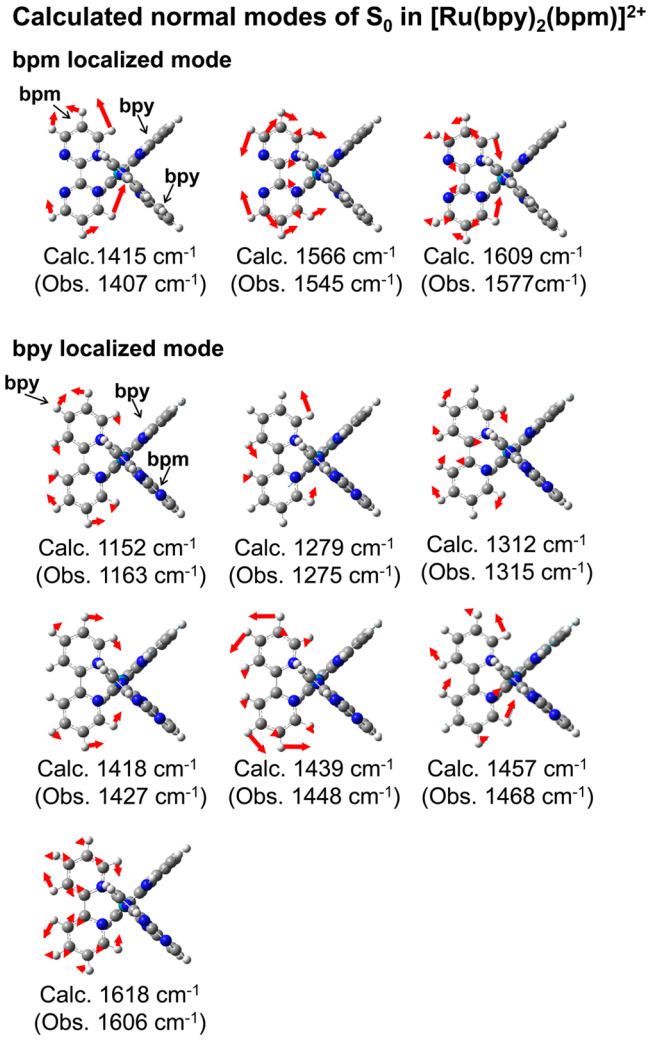

Figure 4. Normal vibrational modes associated with the S_0 state of $[Ru(bpy)_2(bpm)]^{2+}$.

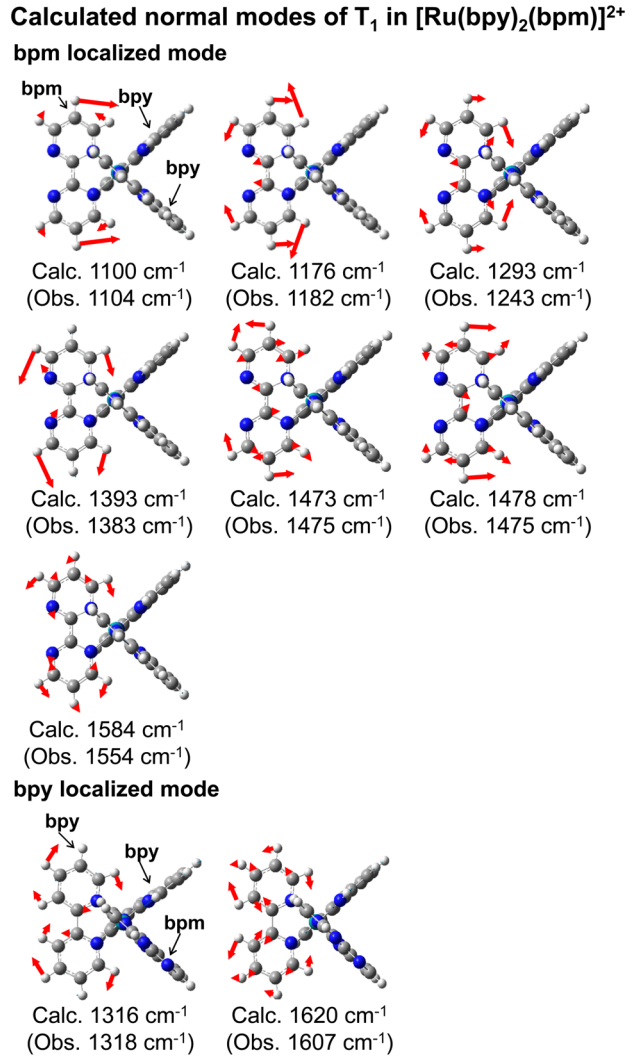

Figure 5. Normal vibrational modes associated with the T_1 state of $[Ru(bpy)_2(bpm)]^{2+}$.

agree well, probably because of imperfect deuteration, as noted in the Materials section.

Figure 3b shows the experimental TR-IR spectrum and the calculated spectrum of the lowest triplet excited state (T_1) of $[Ru(bpy)_2(bpm)]^{2+}$. With the exception of the bleach bands, the transient absorption bands correspond to the transition from $v = 0$ to 1 of the excited triplet state because the population has fully relaxed at the observed delay time of 500 ps. It is thus reasonable to compare the observed transient absorption bands and the calculated bands of T_1. On the basis of the assignments made from deuterium substitution results and the wavenumbers of the bands, we assigned most of the observed bands to the normal vibrational modes of the triplet state, as shown in Figure 5.

The spectral feature that the positive absorption bands are prominent compared to the negative bleach bands in the TR-IR spectra is also reproduced by the calculation. The intensities of the calculated bands in the excited state (approximately 500) are about 5 times as high as those in the ground state (approximately 100), as shown in Figure 3. These intensities are determined by the dipole moment change that accompanies the vibrational transition in each potential. Thus, this difference indicates that reduction of the bpm ligand by metal-to-ligand charge transfer (MLCT) largely deforms the vibrational potentials of bpm in the excited state.

III.1.3. Emergence of the bpy Bands in the Excited Triplet State. Although the major vibrational bands associated with the excited state are assigned to the bpm ligands, there are two exceptions: the bands assigned to the bpy ligand at 1318 and 1607 cm^{-1} shown by the blue circles in Figure 2b. These bands are also well matched by the results of theoretical calculations, as shown by the blue bars in Figure 3b. Moreover, these bands are observed at almost the same wavenumbers, 1315 and 1606 cm^{-1}, in the ground-state spectrum, as shown in Figure 2c. It is noted that the slight energy difference cannot be discussed here because we measured the spectra of the ground and excited states under different conditions, that is, using a KBr pellet and a MeCN solution, respectively. The corresponding normal modes of S_0 (calcd 1312 and 1618 cm^{-1} in Figure 4) and T_1 (calcd 1316 and 1620 cm^{-1} in Figure 5) are also the same, respectively. These results indicate that the transition moments of these modes become significantly larger in the excited state although there is almost no potential change of the bpy ligands due to little charge localization by photoexcitation. Another interesting feature is that the observed intensities of the bands at 1606 cm^{-1} in FT-IR and 1607 cm^{-1} in TR-IR are much

dx.doi.org/10.1021/ic402474t | Inorg. Chem. 2014, 53, 2481−2490

higher than the corresponding calculated intensities, as shown in parts a and b of Figure 3, respectively. The same bands are observed for $[Ru(bpy)_3]^{2+}$, as described in detail later.

III.1.4. Contributions of Molecular Orbitals. Figure 6 shows the selected molecular orbitals related to the excited triplet state

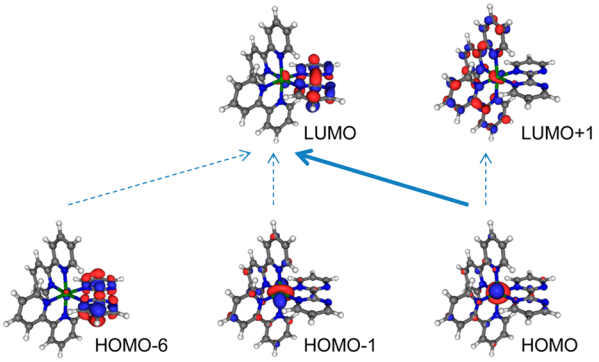

State	Major contribution	[%]
T1 (2.45 eV)	HOMO (Ru) → LUMO (bpm)	70
	HOMO-1 (Ru) → LUMO (bpm)	7
	HOMO (Ru) → LUMO+1 (bpm)	6
	HOMO-6 (bpm) → LUMO (bpm)	5

Figure 6. Contributions of molecular orbitals to the T_1 state of $[Ru(bpy)_2(bpm)]^{2+}$ based on TD-DFT calculations.

(T_1) together with their contributions, as estimated from the TD-DFT calculations. Considering that the calculated vibrational spectra are in good agreement with the experimental spectra, as discussed above, the potentials of the ground state and the lowest triplet state are accurately represented by the calculated values. While the highest occupied molecular orbital (HOMO) and HOMO−1 are primarily centered on the ruthenium atom, the lowest unoccupied molecular orbital (LUMO) and LUMO+1 are localized on the bpm and bpy ligands, respectively. The major contribution of the transition from HOMO to LUMO (70%) clearly shows the transition of orbital localization from the metal to the bpm ligand, indicating that the electron is highly localized on the bpm ligand upon photoexcitation. The charges of the bpy and bpm ligands in the excited triplet state are therefore regarded as neutral (bpy^0) and negative (bpm^{-1}), respectively.

III.2. $[Ru(bpy)_3]^{2+}$. *III.2.1. Vibrational Spectra of the Ground and Excited Triplet States.* $[Ru(bpy)_3]^{2+}$ is the most fundamental ruthenium polypyridyl complex, and thus many studies of its excited state have been carried out.[1−3,42−51] However, to the best of our knowledge, there have been only two reports concerning examination of the excited state using TR-IR.[14,19] One report is a review that presents spectra without analysis,[14] while the other presents step-scan FT-IR spectra, but only over a limited range of wavenumbers (1400−1620 cm^{-1}), and does not contain clear transient absorption bands.[19] The weak IR absorption and complicated vibrational spectra of $[Ru(bpy)_3]^{2+}$ have prevented us from generating detailed assignments of the observed vibrational bands, although we have succeeded in obtaining distinct vibrational spectra in the case of $[Ru(bpy)_2(bpm)]^{2+}$ and have assigned the vibrational bands in those spectra. We therefore applied the same method to the study of the excited state of $[Ru(bpy)_3]^{2+}$ and employed the results obtained for $[Ru(bpy)_2(bpm)]^{2+}$ to assist in analysis of the resulting spectra.

In the analysis of $[Ru(bpy)_2(bpm)]^{2+}$, the vibrational spectrum of $[Ru(bpy)_3]^{2+}$ in the ground state was obtained and is shown in Figure 7a, together with the spectrum of

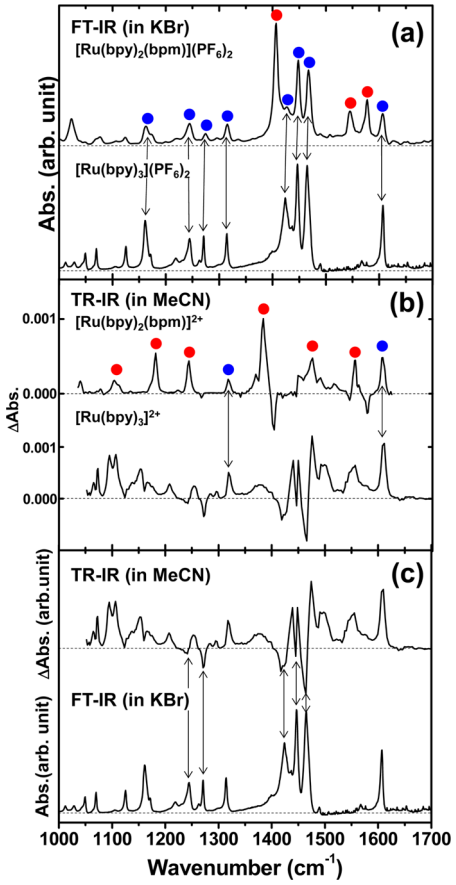

Figure 7. IR vibrational spectra of $[Ru(bpy)_3]^{2+}$ (upper), along with that of $[Ru(bpy)_2(bpm)]^{2+}$ (lower) for comparison purposes: (a) FT-IR spectra of the complexes as KBr pellets; (b) TR-IR spectra of CH_3CN solutions of the complexes 500 ps after photoexcitation with a 400 nm pulse; (c) comparison between the FT-IR and TR-IR spectra of $[Ru(bpy)_3]^{2+}$. Red and blue circles have the same meaning as that in Figure 2.

$[Ru(bpy)_2(bpm)]^{2+}$ for comparison purposes. Considering that all of the ligands of $[Ru(bpy)_3]^{2+}$ are bpy, the intensities and wavenumbers of the spectral bands are in good agreement with the corresponding vibrational bands assigned to the bpy ligands in $[Ru(bpy)_2(bpm)]^{2+}$, indicated by blue solid circles.

Figure 7b shows the transient absorption spectra of $[Ru(bpy)_3]^{2+}$ and $[Ru(bpy)_2(bpm)]^{2+}$ at 500 ps after photoexcitation. The spectrum of $[Ru(bpy)_3]^{2+}$ is more complicated than that of $[Ru(bpy)_2(bpm)]^{2+}$, reflecting its symmetrical structure. In the spectrum of $[Ru(bpy)_2(bpm)]^{2+}$, there are only two vibrational bands, indicated by blue solid circles at 1318 and 1609 cm^{-1}, which are assigned to the bpy ligands. In the spectrum of $[Ru(bpy)_3]^{2+}$, these same locations are indicated by vertical arrows. On the basis of the previous spectral interpretations, these bands are assigned to the neutral bpy ligands (bpy^0). This assignment is in good agreement with the fact that the excited electron of $[Ru(bpy)_3]^{2+}$ is localized on a single bpy ligand (bpy^-).[1−3,52,53] Figure 7c compares the spectra of the ground and excited states. Despite the dense

dx.doi.org/10.1021/ic402474t | Inorg. Chem. 2014, 53, 2481−2490

concentration of vibrational bands, the bleach bands at 1240, 1272, 1419, and 1464 cm^{-1} in the excited-state spectrum are in good agreement with the bands in the ground-state spectrum. The slight wavenumber difference between peaks in the excited- and ground-state spectra is due to the solvation effect.

III.2.2. Normal Vibrational Modes by Quantum Chemical Calculations. In order to assign the observed vibrational bands, we carried out quantum-chemical calculations for $[Ru(bpy)_3]^{2+}$. Similar calculations have already been performed by many groups,[54−57] but the analysis of normal vibrational modes based on such calculations has not been reported. Although a normal-mode analysis has been published,[58,59] it was performed under the assumption that the electron-localized ligands represent anion-radical fragments, which does not always represent a viable model for the excited state. Thus, we carried out the normal-mode analysis based on quantum-chemical calculations using the DFT method, which has been demonstrated to work well for the analysis of $[Ru(bpy)_2(bpm)]^{2+}$. Figure 8a shows

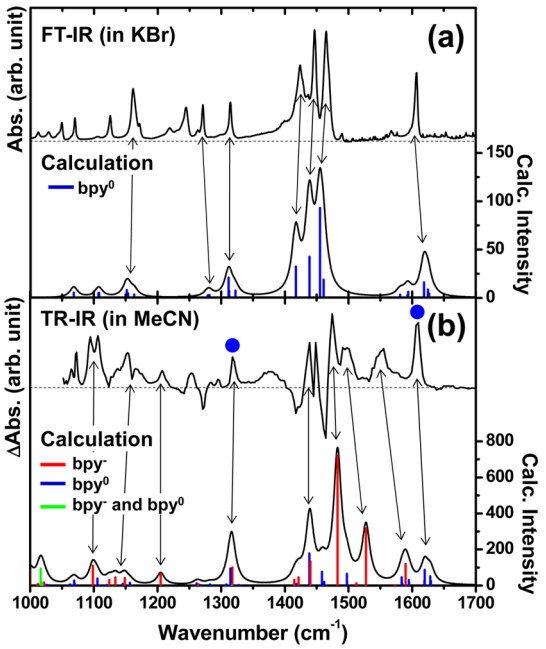

Figure 8. Comparison between the experimental and calculated vibrational spectra of $[Ru(bpy)_3]^{2+}$: (a) experimental FT-IR spectrum (upper) and calculated S_0 state spectrum (lower); (b) experimental TR-IR spectrum (upper) and calculated T_1 state spectrum (lower). The blue circles in the experimental spectrum represent bands associated with vibrations localized on the bpy^0 ligands, based on a comparison with the results obtained for $[Ru(bpy)_2(bpm)]^{2+}$. The bars in the calculated spectra indicate the wavenumbers and intensities of each vibrational mode, while their colors represent the ligand on which the vibrations are localized, judging from the displacement of each normal vibrational mode obtained from calculations (Figures 9 and 10). Blue, red, and green indicate neutral bpy (bpy^0), negatively charged bpy (bpy^-), and both ligands, respectively.

the experimental and calculated vibrational spectra for the ground state, in which the blue bars indicate the wavenumbers and intensities of the vibrational modes obtained from calculations. The vibrational motions obtained from the quantum-chemical calculations are presented in Figure 9.

Figure 8b shows the experimental and calculated vibrational spectra of the excited state. The red and blue bars indicate the wavenumbers and intensities of the localized vibrational modes

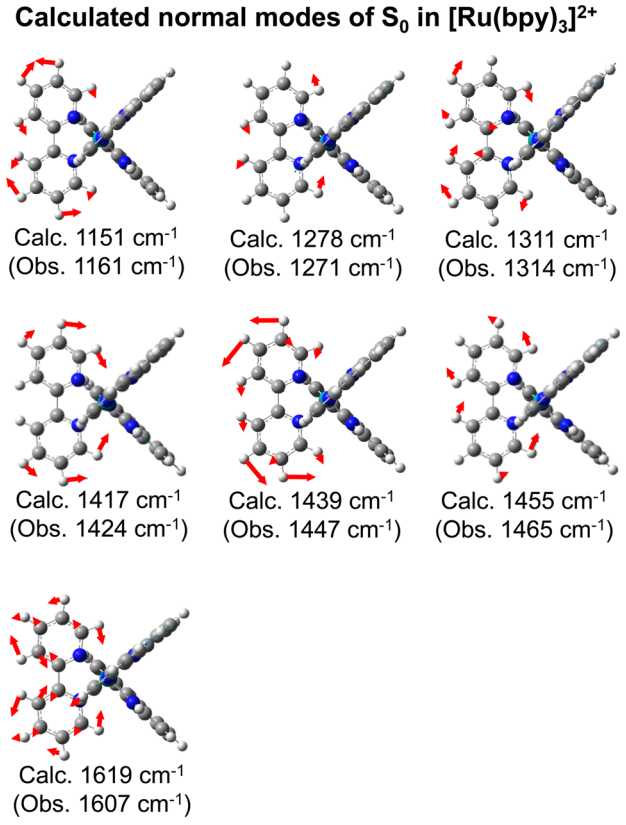

Figure 9. Normal vibrational modes associated with the S_0 state of $[Ru(bpy)_3]^{2+}$.

associated with the electron-localized bpy ligands (bpy^-) and the neutral bpy ligands (bpy^0), respectively, while the green bars represent delocalized modes of both ligands (bpy^- and bpy^0). As discussed above, the experimental spectrum exhibits two special bands assigned to the neutral bpy ligand (bpy^0) at 1318 and 1609 cm^{-1} (indicated by the blue solid circles). These bands are well reproduced in the calculated spectrum, although the band at 1318 cm^{-1} is assigned to two modes of the bpy^0 and bpy^- ligands. In the calculated spectrum, there are more bands assigned to the bpy^0 ligand; however, it is hard to distinguish them because they are overlapped with neighboring strong bpy^- bands. The remaining bands are assigned to the bpy^- ligands. The vibrational motions obtained from the quantum-chemical calculations are shown in Figure 10.

III.2.3. Emergence of the Neutral bpy Bands in the Excited Triplet State. For $[Ru(bpy)_2(bpm)]^{2+}$, the two bands assigned to the neutral bpy ligands at 1318 and 1609 cm^{-1} in the excited state are located at almost the same positions as the bands at 1314 and 1607 cm^{-1} in the ground state, respectively. The normal modes corresponding to these two bands in S_0 (calcd 1311 and 1619 cm^{-1} in Figure 9) and in T_1 (calcd 1315 and 1616 cm^{-1} in Figure 10) are also the same, respectively. Thus, even in $[Ru(bpy)_3]^{2+}$, transition moments of these modes become larger without a potential change by MLCT. Moreover, these vibrational modes are the same as the corresponding modes in $[Ru(bpy)_2(bpm)]^{2+}$ shown in Figures 4 and 5, indicating that the bands located at approximately 1315 or 1605 cm^{-1} in the excited state are assigned to the modes of the neutral bpy ligand independent of the electron-localized ligand (bpy^- or bpm^-).

dx.doi.org/10.1021/ic402474t | Inorg. Chem. 2014, 53, 2481−2490

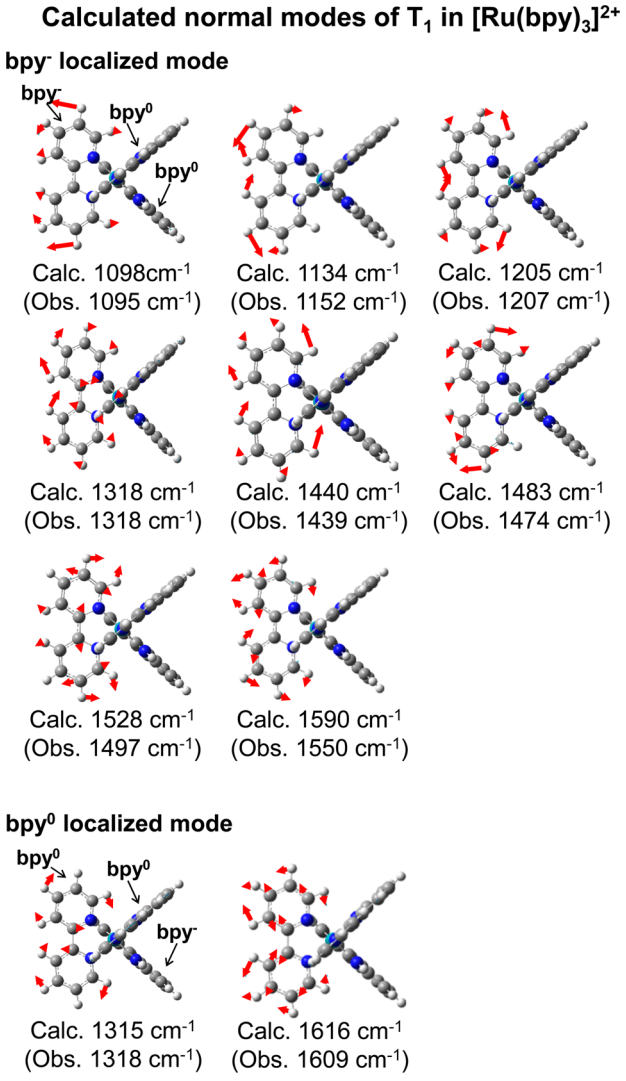

Figure 10. Normal vibrational modes associated with the T_1 state of $[Ru(bpy)_3]^{2+}$.

One of the reasons why only these modes are clearly observed without a potential change by MLCT is probably that they are associated with the ring vibrations. In the mode at approximately 1315 cm^{-1}, the carbon atoms connecting to the two pyridine rings are largely displaced, as shown in the figures of vibrational modes. Especially, in the mode at approximately 1605 cm^{-1}, the four carbon atoms belonging to the pyridine rings are largely displaced. As mentioned in the Introduction, the C═C and C═N stretching vibrations are sensitive to the molecule's charge and structure because of the π-orbital character; thus, these modes would be affected by a slight variation in the charge and structure by MLCT.

The intensity difference of the vibrational bands assigned to the neutral bpy ligands in the ground and excited states of $[Ru(bpy)_3]^{2+}$ was also observed in TR-Raman spectra.[60] They reported that the intensities in the excited state are two-thirds those in the ground states through a comparison of the Raman and TR-Raman spectra. However, these measurements in the ground and excited states were carried out under slightly different conditions, and the intensity difference is independent of the vibrational mode; thus, this is probably a different case of TR-IR. They also reported a wavenumber shift of 6−7 cm^{-1} for specific vibrational modes as a result of oxidation of the central metal in the ground state through a comparison of $[Ru^{II}(bpy)_3]^{2+}$ and $[Ru^{III}(bpy)_3]^{3+}$. This result is more suggestive because it indicates that some specific vibrational modes are affected by oxidation of the central metal without reduction of the bpy ligands, although no information on the intensity difference can be obtained.

We found a difference in the character of the temporal variation of the 1318 and 1609 cm^{-1} bands. Parts a and b of Figure 11 show the spectral changes around the 1318 and 1609

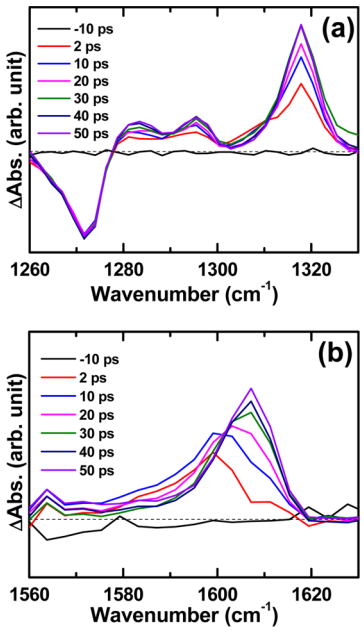

Figure 11. Temporal variations of TR-IR spectra of $[Ru(bpy)_3]^{2+}$ after photoexcitation in the regions (a) from 1260 to 1330 cm^{-1} and (b) from 1560 to 1630 cm^{-1}.

cm^{-1} bands, respectively, up to 50 ps after photoexcitation. In Figure 11a, the intensity of a bleach band at 1272 cm^{-1} does not change, indicating that there is no recovery of the ground state in this time region. The intensity of the 1318 cm^{-1} band gradually increases over 30 ps, indicating that the population of the vibrational ground state ($v = 0$) increases over 30 ps in the excited state. Similar spectral variations are observed in TR-Raman spectra, which are explained by vibrational relaxation in the potential of the excited state.[61] In contrast, only the 1609 cm^{-1} band among all of the observed bands in the region from 1000 to 1700 cm^{-1} exhibits a different temporal variation. As shown in Figure 11b, the central wavenumber of the band increases by 10 cm^{-1} over 50 ps. One possible cause of this shift is a hot band. Higher vibrational states have a smaller transition energy because of anharmonicity; thus, transitions from vibrationally excited states emerge in the lower-wavenumber region. However, this does not conclusively explain the reason why only this band, among many similar vibrational bands, exhibits a wavenumber shift. In general, the wavenumber shift of a vibrational band indicates deformation of the potential due to variation of the charge and/or bond length; thus, the vibrational potential of this band is probably affected by such dynamics because this band is assigned to the mode consisting mainly of ring vibrations that are sensitive to charge and structure variations.

As shown here, the relatively slow dynamics on the tens of picoseconds time scale including vibrational relaxation in the

dx.doi.org/10.1021/ic402474t | Inorg. Chem. 2014, 53, 2481−2490

excited states has not been clearly understood yet. Because the dynamics is directly connected with photochemical reactions in ruthenium polypyridyl complexes, further studies using TR-IR or other methods are required.

III.2.4. Contributions of Molecular Orbitals. The selected molecular orbitals and transitions in the T_1 state calculated by DFT and TD-DFT methods are shown in Figure 12. The major

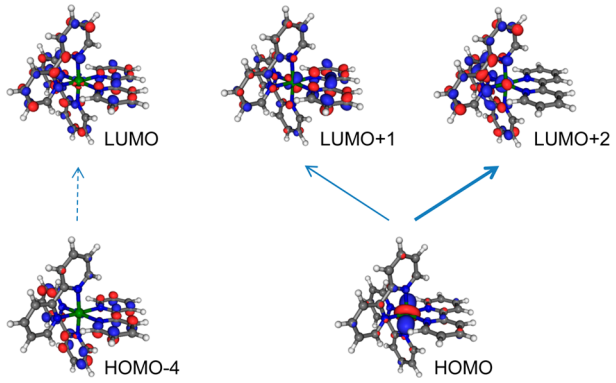

State	Major contribution	[%]
T1 (2.54 eV)	HOMO (Ru) → LUMO+2 (bpy)	42
	HOMO (Ru) → LUMO+1 (bpy)	25
	HOMO-4 (bpy) → LUMO (bpy)	5

Figure 12. Contributions of molecular orbitals to the T_1 state of $[Ru(bpy)_3]^{2+}$ based on TD-DFT calculations.

contribution (42%) is from the HOMO to LUMO+2 transition, indicating charge transfer from the metal to the two bpy ligands. The second contribution (25%) is from the HOMO to LUMO+1 transition, which corresponds to charge transfer from the metal to the three bpy ligands but is slightly one-sided on the one ligand that is not included in the LUMO +2. An excited electron is considered to distribute the three bpy ligands unevenly in these transitions. This explains the empirical observation that the normal vibrational modes are classified into two types: one type that is localized on two bpy ligands and the other bpy ligand. However, the charge in this compound is not as highly localized at the single ligand compared to $[Ru(bpy)_2(bpm)]^{2+}$.

IV. CONCLUSION

We have comprehensively investigated the IR vibrational spectra over the range of 1000−1700 cm^{-1} in the ground and excited states of heteroleptic $[Ru(bpy)_2(bpm)]^{2+}$ and prototypical homoleptic $[Ru(bpy)_3]^{2+}$ using FT-IR and TR-IR. By deuterium substation and quantum-chemical calculation, we assigned almost all of the observed bands to the calculated normal modes. These results are in good agreement with the well-known model in which the excited electron is localized at a single ligand (bpm^- or bpy^-). Moreover, we found two vibrational bands assigned to the neutral bpy ligands (bpy^0) at approximately 1317 and 1608 cm^{-1} without a large wavenumber shift, and these bands are commonly observed in $[Ru(bpy)_2(bpm)]^{2+}$ and $[Ru(bpy)_3]^{2+}$. This is probably because these modes include ring vibrations that are sensitive to the charge and structural variations of molecules and oxidation of the ruthenium by MLCT affects such modes. We also found that the 1609 cm^{-1} band in $[Ru(bpy)_3]^{2+}$ exhibits wavenumber shifts over 50 ps, probably because this mode is especially sensitive to charge and structural changes. These detailed assignments of IR vibrational bands in the ground and excited states will be helpful for analyzing the dynamics of many photofunctional materials using ruthenium polypyridyl complexes. We are currently pursuing these research endeavors.

■ ASSOCIATED CONTENT

Supporting Information

NMR data, plot of the absorbance change of vibrational bands in a TR-IR spectrum, a comparison of the calculated spectra, and Cartesian coordinates. This material is available free of charge via the Internet at http://pubs.acs.org.

■ AUTHOR INFORMATION

Corresponding Author

*E-mail: onda.k.aa@m.titech.ac.jp. Phone/fax: +81-45-924-5891.

Notes

The authors declare no competing financial interest.

■ ACKNOWLEDGMENTS

This study was supported by the JST, PRESTO (Precursory Research for Embryonic Science and Technology), the G-COE program of the Tokyo Institute of Technology (funded by the Japan Society for the Promotion of Science, JSPS), and a Grant-in-Aid for JSPS Fellows (to K.M.). K.M. thanks Prof. Dr. Jean-François Halet and Dr. Karine Costuas (Université de Rennes 1, Rennes, France) for the helpful discussions on DFT calculations. Calculations were performed on TSUBAME 2.0, a supercomputer at the Tokyo Institute of Technology, which is gratefully acknowledged.

■ REFERENCES

(1) Thompson, D. W.; Ito, A.; Meyer, T. J. *Pure Appl. Chem.* **2013**, *85*, 1257.
(2) Campagna, S.; Puntoriero, F.; Nastasi, F.; Bergamini, G.; Balzani, V. *Top. Curr. Chem.* **2007**, *280*, 117.
(3) Juris, A.; Balzani, V.; Barigelletti, F.; Campagna, S.; Belser, P.; Von Zelewsky, A. *Cood. Chem. Rev.* **1988**, *84*, 85.
(4) Inagaki, A.; Akita, M. *Coord. Chem. Rev.* **2010**, *254*, 1220.
(5) Concepcion, J. J.; Jurss, J. W.; Brennaman, M. K.; Hoertz, P. G.; Patrocinio, A. O. T.; Iha, N. Y. M.; Templeton, J. L.; Meyer, T. J. *Acc. Chem. Res.* **2009**, *42*, 1954.
(6) Doherty, M. D.; Grills, D. C.; Muckerman, J. T.; Polyansky, D. E.; Fujita, E. *Coord. Chem. Rev.* **2010**, *254*, 2472.
(7) Graetzel, M. *Acc. Chem. Res.* **2009**, *42*, 1788.
(8) O'Regan, B.; Graetzel, M. *Nature* **1991**, *335*, 737.
(9) Terpetschnig, E.; Szmacinski, H.; Malak, H.; Lakowicz, J. R. *Biophys. J.* **1995**, *68*, 342.
(10) Montalti, M.; Wadhwa, S.; Kim, W. Y.; Kipp, R. A.; Schmehl, R. H. *Inorg. Chem.* **2000**, *39*, 76.
(11) Prier, C. K.; Rankic, D. A.; Macmillan, D. W. C. *Chem. Rev.* **2013**, *113*, 5322.
(12) Yoon, T. P.; Ischay, M. A.; Du, J. *Nat. Chem.* **2010**, *2*, 527.
(13) Nicewicz, D.; MacMillan, D. W. C. *Science* **2008**, *332*, 77.
(14) Butler, J. M.; George, M. W.; Shoonover, J. R.; Dattelbaum, D. M.; Meyer, T. J. *Coord. Chem. Rev.* **2007**, *251*, 492.
(15) Schoonover, J. R.; Bignozzi, C. A.; Meyer, T. J. *Coord. Chem. Rev.* **1997**, *165*, 239.
(16) Matsubara, Y.; Okimoto, Y.; Yoshida, T.; Ishikawa, T.; Koshihara, S.; Onda, K. *J. Phys. Soc. Jpn.* **2011**, *80*, 124711.
(17) Fukazawa, N.; Shimizu, M.; Ishikawa, T.; Okimoto, Y.; Koshihara, S.; Hiramatsu, T.; Nakano, Y.; Yamochi, H.; Saito, G.; Onda, K. *J. Phys. Chem. C* **2012**, *116*, 5892.

(18) Fukazawa, N.; Tanaka, T.; Ishikawa, T.; Okimoto, Y.; Koshihara, S.; Yamamoto, T.; Tamura, M.; Kato, R.; Onda, K. *J. Phys. Chem. C* **2013**, *117*, 13187.
(19) Omberg, K. M.; Schoonover, J. R.; Treadway, A.; Leasure, R. M.; Dyer, R. B.; Meyer, T. J. *J. Am. Chem. Soc.* **1997**, *119*, 7013.
(20) Omberg, K. M.; Schoonover, J. R.; Bernhard, S.; Moss, J. A.; Treadway, J. A.; Kober, E. M.; Dyer, R. B.; Meyer, T. J. *Inorg. Chem.* **1998**, *37*, 3505.
(21) Curtright, A. E.; McCusker, J. K. *J. Phys. Chem. A* **1999**, *103*, 7032.
(22) Alsindi, W. Z.; Easun, T. L.; Sun, X.-Z.; Ronayne, K. L.; Towrie, M.; Herrera, J.-M.; George, M. W.; Ward, M. D. *Inorg. Chem.* **2007**, *46*, 3696.
(23) Li, G.; Parimal, K.; Vyas, S.; Hadad, C. M.; Flood, A. H.; Glusac, K. D. *J. Am. Chem. Soc.* **2009**, *131*, 11656.
(24) Easun, T. L.; Alsindi, W. Z.; Deppermann, N.; Towrie, M.; Ronayne, K. L.; Sun, X. -Z.; Ward, M. D.; George, M. W. *Inorg. Chem.* **2009**, *48*, 8759.
(25) Sato, S.; Matubara, Y.; Koike, K.; Falkenström, M.; Katayama, T.; Ishibashi, Y.; Miyasaka, H.; Taniguchi, S.; Chosrowjan, H.; Mataga, N.; Fukazawa, N.; Koshihara, S.; Onda, K.; Ishitani, O. *Chem.—Eur. J.* **2012**, *18*, 15722.
(26) Murata, K.; Araki, M.; Inagaki, A.; Akita, M. *Dalton Trans.* **2013**, *42*, 6989.
(27) Esaki, H.; Ito, N.; Sakai, S.; Maegawa, T.; Monguchi, Y.; Sajiki, H. *Tetrahedron* **2006**, *62*, 10954.
(28) Kogon, I. C; Minin, R.; Overberger, C. G.. *Org. Synth.* **1963**, *4*, 182.
(29) Schwab, P. F. H.; Fleischer, F.; Michl, J. J. *Org. Chem.* **2002**, *67*, 443.
(30) Browne, W. R.; O'Connor, C. M.; Killeen, J. S.; Guckian, A. L.; Burke, M.; James, P.; Burke, M.; Vos, J. G. *Inorg. Chem.* **2002**, *41*, 4245.
(31) Sullivan, B. P.; Salmon, D. J.; Meyer, T. J. *Inorg. Chem.* **1977**, *17*, 3334.
(32) Ji, Z.; Huang, S. D.; Guadalupe, A. R. *Inorg. Chim. Acta* **2000**, *305*, 127.
(33) Inagaki, A.; Yatsuda, S.; Edure, S.; Suzuki, A.; Takahashi, T.; Akita, M. *Inorg. Chem.* **2007**, *46*, 2432.
(34) Frisch, M. J.; Trucks, G. W.; Schlegel, H. B.; Scuseria, G. E.; Robb, M. A.; Cheeseman, J. R.; Scalmani, G.; Barone, V.; Mennucci, B.; Petersson, G. A.; et al. *Gaussian 09*, revision A.2; Gaussian Inc.: Wallingford, CT, 2009.
(35) Adamo, C.; Barone, V. J. *Chem. Phys.* **1998**, *108*, 664.
(36) Dunning, T. H.; Hay, P. J. In *Modern Theoretical Chemistry*; Schaefer, H. F., III, Ed.; Plenum: New York, 1976; Vol. 3, p 1.
(37) Wadt, W. R.; Hay, P. J. *J. Chem. Phys.* **1985**, *82*, 284.
(38) Tomasi, J.; Mennucci, B.; Cammi, R. *Chem. Rev.* **2005**, *105*, 2999.
(39) Wadt, W. R.; Hay, P. J. *J. Chem. Phys.* **1985**, *82*, 299.
(40) Varetto, U. *Molekel 5.4*; Swiss National Supercomputing Centre: Lugano, Switzerland, 2009.
(41) Rillema, D. P.; Mack, K. B. *Inorg. Chem.* **1982**, *21*, 3849.
(42) Malone, R. A.; Kelly, D. F. *J. Chem. Phys.* **1991**, *95*, 8970.
(43) Damrauer, N. H.; Cerullo, G.; Yeh, A.; Boussie, T. R.; Shank, C. V.; McCusker, J. K. *Science* **1997**, *275*, 54.
(44) Yeh, A. T.; Shank, C. V.; McCusker, J. K. *Science* **2000**, *289*, 935.
(45) Bhasikuttan, A. C.; Suzuki, M.; Nakashima, S.; Okada, T. *J. Am. Chem. Soc.* **2002**, *124*, 8398.
(46) McCusker, J. K. *Acc. Chem. Res.* **2003**, *36*, 876.
(47) Wallin, S.; Davidsson, J.; Modin, J.; Hammarström, H. *J. Phys. Chem. A* **2005**, *109*, 4697.
(48) Cannizzo, A.; van Mourik, F.; Gawelda, W.; Zgrablic, G.; Bressler, C.; Chergui, M. *Angew. Chem., Int. Ed.* **2006**, *45*, 3179.
(49) Sato, T.; Nozawa, S.; Tomita, A.; Hoshino, M.; Koshihara, S.; Fujii, H.; Adachi, S. *J. Phys. Chem. C* **2012**, *116*, 14232.
(50) Henry, W.; Coates, C. G.; Brady, C.; Ronayne, K. L.; Matousek, P.; Towrie, M.; Botchway, S. W.; Parker, A. W.; Vos, J. G.; Browne, W. R.; McGarvey, J. J. *J. Phys. Chem. A* **2008**, *112*, 4537.
(51) Su, Q.; Mosquera-Vazquez, S.; Daku, L. M. L.; Guenee, L.; Goodwin, H. A.; Vauthey, E.; Hauser, A. *J. Am. Chem. Soc.* **2013**, *135*, 13660.
(52) Carroll, P. J.; Brus, L. E. *J. Am. Chem. Soc.* **1987**, *109*, 7613.
(53) McCusker, C. E.; McCusker, J. K. *Inorg. Chem.* **2011**, *50*, 1656.
(54) Nozaki, K.; Takamori, K.; Nakatsugawa, Y.; Ohno, T. *Inorg. Chem.* **2005**, *45*, 6161.
(55) Baranovski, V. I.; Lubimova, O. O. *Int. J. Quantum Chem.* **2004**, *96*, 116.
(56) Daul, C.; Baerends, E. J.; Vernooijs, P. *Inorg. Chem.* **1994**, *33*, 3538.
(57) Kober, E. M.; Meyer, T. J. *Inorg. Chem.* **1984**, *23*, 3877.
(58) Schönherr, T.; Degen, J.; Gallhuber, E.; Hensler, G.; Yersin, H. *Chem. Phys. Lett.* **1989**, *158*, 519.
(59) Strommen, D. P.; Mallick, P. K.; Danzer, G. D.; Lumpkin, R. S.; Kincaid, J. R. *J. Phys. Chem.* **1990**, *94*, 1357.
(60) Bradly, P. G.; Kress, N.; Hornberer, B. A.; Dallinger, R. F.; Woodruff, W. H. *J. Am. Chem. Soc.* **1981**, *103*, 7441.
(61) Henry, W.; Coates, C. G.; Brady, C.; Ronayne, K. L.; Matousek, P.; Towrie, M.; Botchway, S. W.; Parker, A. W.; Vos, J. G.; Browne, W. R.; McGarvey, J. J. *J. Phys. Chem. A* **2008**, *112*, 4537.